ASME Journal of Tribology
Online journal at:
https://asmedigitalcollection.asme.org/tribology

Shenglin Liang
College of Mechanical and Electrical Engineering;
National Key Laboratory of Helicopter Aeromechanics,
Nanjing University of Aeronautics and Astronautics,
Nanjing 210016, China
e-mail: Liangsl@nuaa.edu.cn

Qingwen Dai
College of Mechanical and Electrical Engineering;
National Key Laboratory of Helicopter Aeromechanics,
Nanjing University of Aeronautics and Astronautics,
Nanjing 210016, China
e-mail: daiqingwen@nuaa.edu.cn

Wei Huang[1]
College of Mechanical and Electrical Engineering;
National Key Laboratory of Helicopter Aeromechanics,
Nanjing University of Aeronautics and Astronautics,
Nanjing 210016, China
e-mail: huangwei@nuaa.edu.cn

Xiaolei Wang
College of Mechanical and Electrical Engineering;
National Key Laboratory of Helicopter Aeromechanics,
Nanjing University of Aeronautics and Astronautics,
Nanjing 210016, China;
Nanjing University of Aeronautics and Astronautics,
Nanjing 210016, China
e-mail: xlwanggo163@163.com

MoS_2/Ti Co-Deposited Coatings and Their Fretting Wear Properties at Elevated Temperatures

Fretting wear refers to the damage phenomenon experienced by the mechanical components undergoing micro-amplitude relative slip at their contact region due to vibration. Titanium alloys find their extensive application in aerospace industry components such as splines and dovetail joints, where they experience fretting wear phenomenon. This research work investigates the effect of MoS_2/Ti co-deposition coatings with varying Ti contents, deposited on the TC4 titanium alloy substrate using magnetron sputtering. Fretting wear tests were conducted at room temperature, 100 °C, and 200 °C, using a specially designed fretting test fixture with a ball-on-flat contact configuration, mounted on a servo-hydraulic fatigue testing machine. The results indicated that the coating becomes denser with an increase in the Ti content. The coating exhibited the highest hardness and better anti-fretting wear performance at room temperature. However, the effect of Ti content on the fretting wear behaviors changed at elevated temperatures. At the highest Ti content coating, excessive oxide particles were found on the worn surface at elevated temperatures, inducing an abrasive effect and localized cracks. However, coatings with moderate Ti content (9.62 at%) effectively protected the substrate from significant wear at room temperature and maintained a low coefficient of friction at high temperatures without failure. [DOI: 10.1115/1.4067042]

Keywords: MoS_2/Ti composite coating, magnetron sputtering, fretting wear, TC4 alloys, high temperature, abrasion, coatings, friction

1 Introduction

Titanium alloys, especially TC4, find their wide application in several industries including aerospace and naval, due to their attractive mechanical properties like high strength-to weight ratio and good corrosion resistance. However, like other light metals, such as aluminum and magnesium alloy, they exhibit inferior tribological properties [1,2]. Fretting wear phenomenon is experienced by several mechanical components in aerospace industry like transmission splines and turbine engine disk and blade dovetail joints. The relative slip of micro-amplitude between the mating surfaces due to vibration results in fretting wear and other damage phenomenon, leading to transmission system failures [3–6]. Therefore, adequate treatments must be taken to improve the fretting wear resistance of the titanium alloy parts. Several methods have been applied by the researchers to improve the fretting wear performance including shot peening [7–9], rolling [10,11], micro-arc oxidation [12,13], and solid lubrication coatings [14–16].

Molybdenum disulfide (MoS_2), a typical two-dimensional material with an S–Mo–S sandwich structure, has drawn great attention in recent years due to its unique physicochemical properties [17–20]. MoS_2 coatings prepared by physical vapor deposition (PVD), notably magnetron sputtering, leverage the technical merits inherent in vacuum sputtering techniques [21]. These coatings demonstrate exceptional uniformity, robust adhesion, and enhanced stability [22,23], rendering them highly effective in lubrication under severe conditions, including nitrogen atmospheres and vacuum

[1]Corresponding author.

Contributed by the Tribology Division of ASME for publication in the JOURNAL OF TRIBOLOGY. Manuscript received August 16, 2024; final manuscript received October 18, 2024; published online November 26, 2024. Tech. Editor: Robert L. Jackson.

environments [24]. Xu et al. [16] deposited MoS_2 coatings on 1045 steel substrates using radio frequency (RF) sputtering after ion-plated tin and shot peening pretreatment. They found that the fretting wear performance of MoS_2 coatings is correlated with the properties of the substrate. Yin et al. [25] investigated the fretting wear behavior of MoS_2 films deposited on AISI 304 stainless steel and found that their lamellar structure, which promotes slip and plastic flow mechanisms, contributes to achieving low friction and wear. However, many researchers [26–29] have demonstrated that the surface of pure MoS_2 coating exhibits porous structures, which are prone to react with moisture and oxygen in the atmospheric environment, to form MoO_3. This severely limits its applications due to the reduction in load-bearing capacity and wear resistance.

To overcome the issue of loose coating structure and oxidation, elemental doping methods are usually employed, and the elements of Ti, Au, Pb, and Al are the common choice [30–34]. The doped metal element can inhibit the grain growth of MoS_2. Therefore, the density of MoS_2 coating increases while the porosity of the coating decreases as well. As a result, the oxidation behavior of MoS_2 in atmospheric environments can be suppressed effectively. Lu et al. [35] used multi-target magnetron co-sputtering method to fabricate MoS_2–(Cr, Nb, Ti, Al, V) composite coatings with varying metals doping. It was found that the higher doping levels improved the density and the tribological properties of the coatings. Hu et al. [36] investigated variation in Ti contents in MoS_2/Ti coatings using magnetron sputtering, leading to enhanced hardness, elastic modulus, and wear resistance. Serpini et al. [37] investigated the tribological behavior of RF magnetron sputtering MoS_2 films by using a ball-on-disc tester at different humidities and temperatures. They found that water may cause the deterioration of the lubricating properties of the films, and film oxidation plays only a marginal role.

However, a few researchers [16,36] have also investigated the fretting wear of MoS_2/Ti composite coatings with Ti doping. Can excellent anti-fretting wear be achieved with increased Ti contents, and what is the corresponding wear mechanism at elevated temperatures? There is not much literature available about this phenomenon. In this research work, MoS_2/Ti co-deposited coatings with varying Ti contents were deposited on TC4 titanium alloy substrates, using magnetron sputtering technology. The coating was also deposited on the silicon wafer to facilitate the acquisition of cross-sectional SEM images. The composition, morphology, hardness, and elastic modulus of the coatings were investigated. More attention was paid to the fretting wear behaviors of the coatings at different temperatures.

2 Experimental Procedures

2.1 Fabrication. The pure MoS_2 coating and MoS_2/Ti composite coating were deposited on TC4 titanium alloy and silicon wafers (for capturing cross-sectional SEM images), using a closed-field unbalanced magnetron sputtering system. Figure 1 illustrates the principle of magnetron sputtering. High-purity targets of MoS_2 (purity: 99.99%) and Ti (purity: 99.99%) were employed for the sputtering. RF magnetron sputtering was utilized for the MoS_2 target, while DC magnetron sputtering was applied for the Ti target. The distance between the target and substrate was fixed at 10 cm. Before deposition, the TC4 titanium alloy substrate underwent meticulous polishing to achieve a mirror-like surface, followed by sequential ultrasonic cleaning in acetone and anhydrous ethanol for 20 min each. Additionally, a Ti interlayer was deposited on the substrate via DC magnetron sputtering to enhance the adhesion between the final coating and the substrate. The specific deposition process consisted of the following steps: first, the high-purity argon was introduced as a working gas, after the chamber reached the vacuum of 1×10^{-3} Pa and the substrate underwent a 30 min glow-cleaning process, using a Hall ion source to eliminate oxides and other impurities. Then, the DC magnetron power supply was engaged, and a titanium interlayer was deposited over 20 min. Finally, the RF and DC power supplies were activated simultaneously for co-sputter deposition. The flowrate of argon was maintained at 30 cm^3/min. The DC power supply was adjusted to achieve the deposition of MoS_2/Ti composite coatings with varying Ti contents. Detailed parameters can be found in Table 1.

The cross-sectional appearance of the coatings was observed by a scanning electron microscope (SEM) equipped with an energy-dispersive spectrometer (EDS) (QUANTAX 200, Bruker, US).

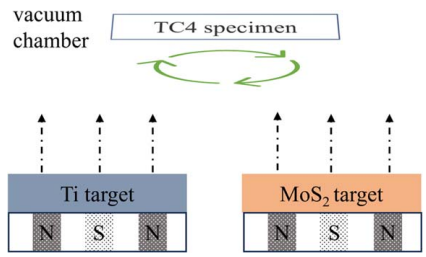

Fig. 1 Schematic diagram of the coating deposition system

Table 1 Deposition parameters of the MoS_2/Ti composite coatings

Procedure Sample	Ar ($cm^3 \cdot min^{-1}$)	Power (W) Ti	Power (W) MoS_2	Temperature (°C)	Deposition time (min)
Ti Interlayer	50	210	0	150	20
Pure MoS_2	30	0	200	150	120
MoS_2/Ti-1	30	25	200	150	150
MoS_2/Ti-2	30	50	200	150	180
MoS_2/Ti-3	30	100	200	150	240

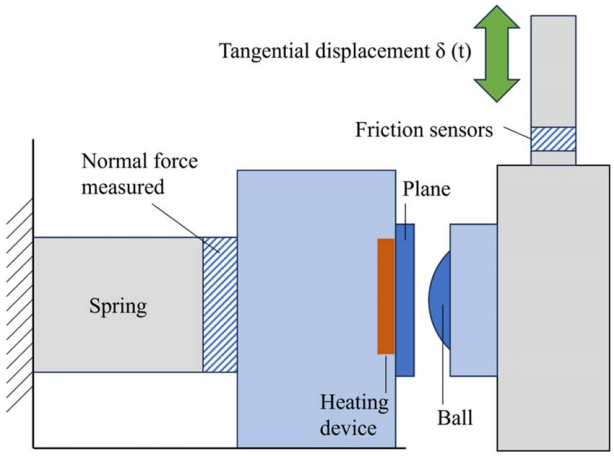

Fig. 2 Fretting wear test fixture

Table 2 The composition and thickness of MoS_2/Ti composite coatings

Sample	Atomic percentage (at%) Mo	S	Ti	Thickness (μm)
Pure MoS_2	29.51	67.18	3.31	3.8 ± 0.05
MoS_2/Ti-1	30.30	62.27	7.43	3.7 ± 0.05
MoS_2/Ti-2	28.75	61.63	9.62	3.4 ± 0.05
MoS_2/Ti-3	19.19	47.51	33.30	3.1 ± 0.05

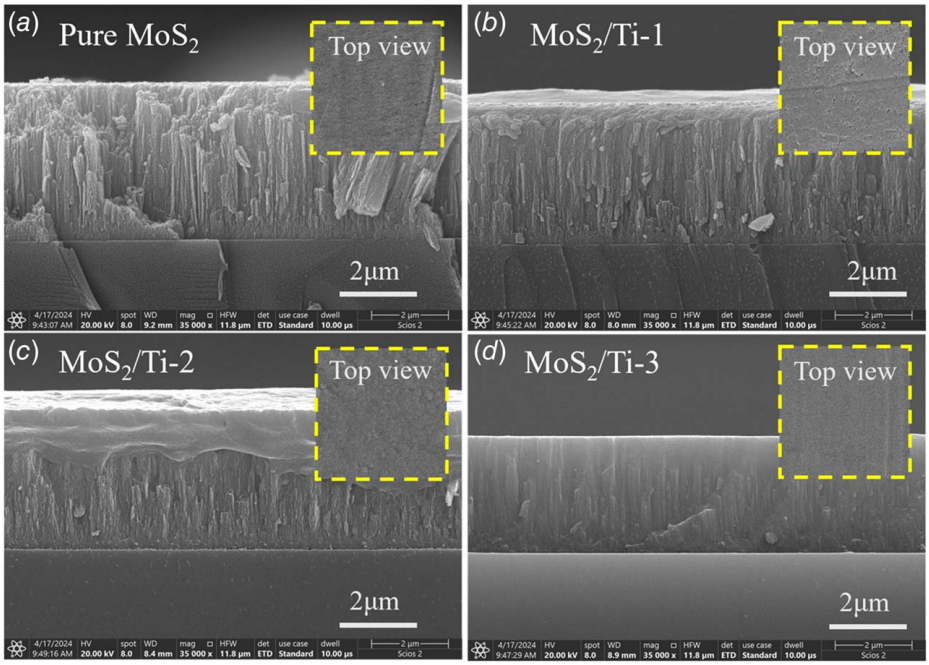

Fig. 3 The SEM micrographs: (*a*) MoS_2, (*b*) MoS_2/Ti-1, (*c*) MoS_2/Ti-2, and (*d*) MoS_2/Ti-3 coatings

Hardness can be regarded as a resistance to material's plastic deformation, and it is also closely related to wear resistance. Thus, the hardness H and elastic modulus E of the coatings were evaluated using a nano-indenter G200 (KLA-Tencor Co. Ltd.) equipped with a Berkovich-type diamond indenter. To eliminate the effect of the substrate, the indentation depth was fixed at about 300 nm, which was less than one-tenth of the coating thickness. Each sample was measured five times to ensure the reliability of the data.

2.2 Experiment and Characterization. Fretting wear tests were carried out using a specially designed test fixture having a ball-on-flat contact configuration and capable of testing at various temperatures, as depicted in Fig. 2. This fixture was mounted on a servo-hydraulic fatigue testing machine, which actuated the ball to generate displacement. At the same time, the surface temperature of the specimen was regulated by a pre-buried ceramic plate below the substrate (temperature measured using a J-type thermocouple with a sensitivity of ±0.5 °C). A TC4 ball with a diameter of Φ10 mm was selected as the counterpart. The displacement amplitude was maintained at 50 μm and the normal load (preload) of 20 N was applied, corresponding to the Hertzian contact stress of 863.1 MPa. The frequency was kept constant at 10 Hz, with the fretting wear cycle of 10,000. Experiments were conducted at room temperature, 100 °C, and 200 °C, respectively. Each experiment was repeated at least three times to determine the repeatability of the friction and wear data.

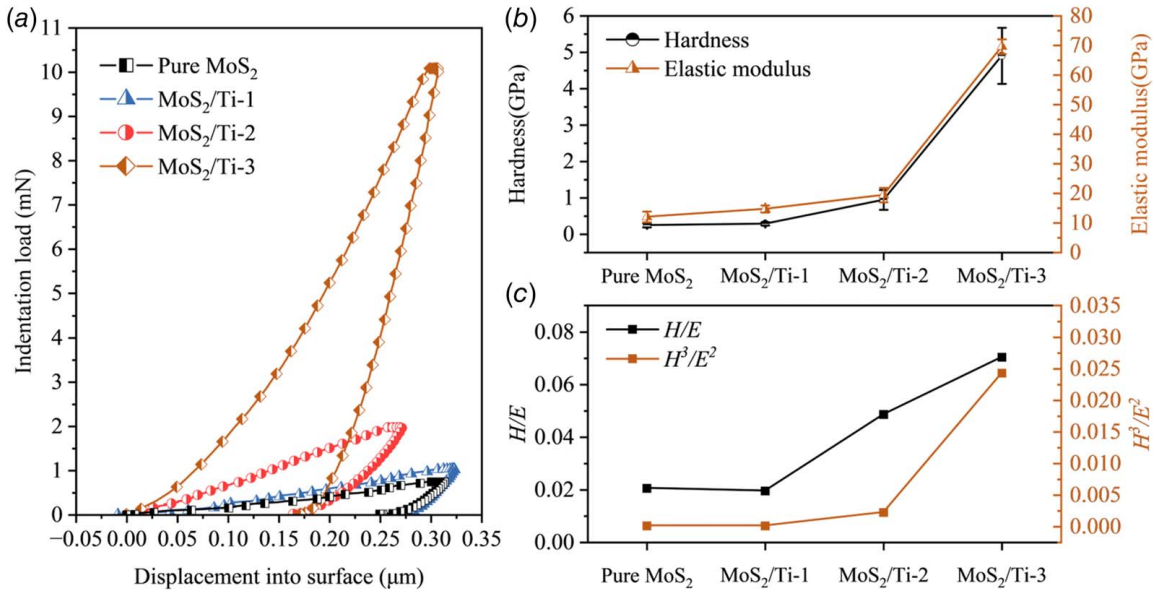

Fig. 4 (*a*) Nano-indentation load versus indentation displacement curves for the coatings, (*b*) hardness (H) and elastic modulus (E), and (c) H/E and H^3/E^2

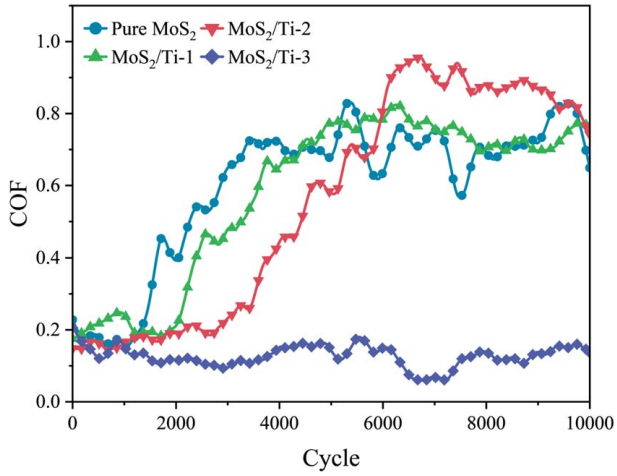

Fig. 5 Variation in COF for the four coatings at room temperature

After the fretting wear tests, the worn surface was evaluated by SEM, and the volumetric material loss was measured using a 3D profilometry (Contour GT, Bruker, USA) in the VSI model (an objective with a magnification of 2.5). The wear-rate was estimated by dividing the wear volume loss by the normal load and sliding distance. Moreover, Raman spectroscopy (LabRAM HR Evolution, Horiba, France) with a 532 nm Ar + laser was employed to analyze the wear debris composition on the worn surface.

3 Results and Discussion

3.1 Compositions and Morphologies. Table 2 presents the chemical composition and thickness of pure MoS_2 and MoS_2/Ti composite coatings. A certain amount of Ti element was also found in pure MoS_2 specimens. Due to the sputtering of the Ti intermediate layer, a small amount of Ti remaining in the vacuum chamber body participates in the subsequent sputtering process of MoS_2 coating.

Based on Tables 1 and 2, it was observed that the thickness of the pure MoS_2 and MoS_2/Ti-1 coatings was closer, while the specimen with the highest Ti content (MoS_2/Ti-3) needed a longer depositing time and exhibited the least thickness. This phenomenon exhibits that the doping Ti element may enhance the compactness of the MoS_2/Ti composite coatings.

Figure 3 shows the cross-sectional morphologies of the MoS_2 and MoS_2/Ti composite coatings. The columnar structure of the pure MoS_2 coating was observed to be relatively loose and susceptible to damage under external forces. Moreover, oxygen and water molecules in the air can easily enter the interstitial lattice, resulting in a serious oxidation phenomenon [38]. In contrast, with the increase of Ti content, the cross-sectional structures as well as the surfaces of MoS_2/Ti composite coatings became denser and smoother. While the orientation consistency of the columnar structure also improved. Similar results have been reported in previous studies [36,39].

3.2 Hardness and Elastic Modulus. Figure 4(*a*) presents the nano-indentation load versus indentation displacement curves of the coatings. According to the standard Oliver and Pharr approach (Eqs. (1)–(4)) [40], the contact area between the indenter and the tested material during indentation (A_c) and the elastic contact stiffness (S) can be calculated.

$$P = B(h - h_f)^m \tag{1}$$

where B and m are the fitting parameters obtained by measurement and h_f is the displacement after complete unloading.

$$S = \left(\frac{dP}{dH}\right)_{h=h_{\max}} = B(h_{\max} - h_f)^{m-1} \tag{2}$$

$$h_c = h_{\max} - \varepsilon \frac{P_{\max}}{S} \tag{3}$$

Here, ε is a constant dependent on the shape of the indenter; h_c is the contact depth, and $h_{\max}$ is the maximum indentation depth.

$$A_c = f(h_c) \tag{4}$$

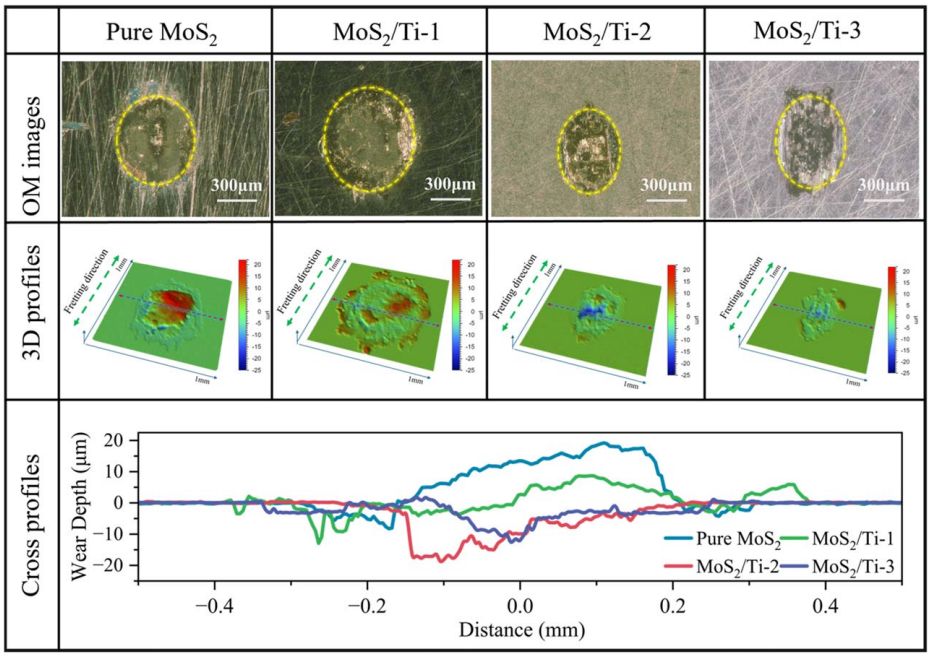

Fig. 6 The optical microscope (OM) images, 3D, and cross-sectional profiles of the wear scars observed for the four coatings, under room temperature

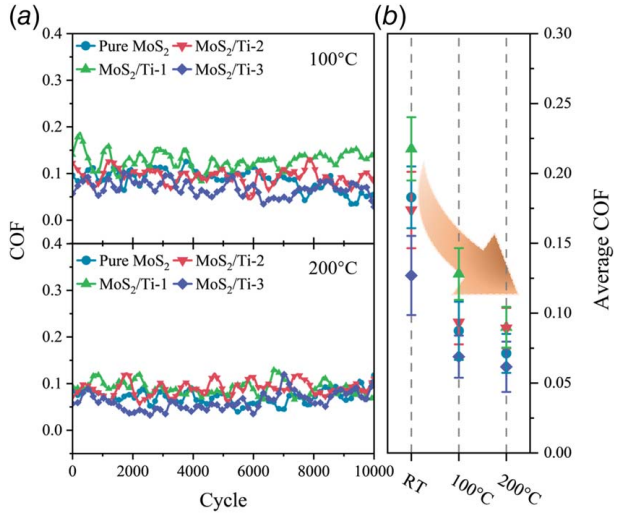

Fig. 7 Variation in COF for the four coatings: (*a*) at 100 °C and 200 °C and (*b*) average COF at different temperatures

The hardness and elastic modulus of the coating can be calculated by using A_c and S in Eqs. (5)–(7).

$$H = \frac{P_{\max}}{A_c} \tag{5}$$

$$E_r = \frac{\sqrt{\pi}}{2\beta}\frac{S}{\sqrt{A_c}} \tag{6}$$

$$\frac{1}{E_r} = \frac{1-\nu^2}{E} + \frac{1-\nu_i^2}{E_i} \tag{7}$$

Here, β is related to the shape of the indenter and E_r represents the reduced elastic modulus, used to account for the elastic deformation of the specimen. E and ν are the elastic modulus and Poisson's ratio of the tested material, respectively, E_i and ν_i are the elastic modulus and Poisson's ratio of the indenter, respectively.

The mean values of hardness (H) and elastic modulus (E) for the MoS_2/Ti coatings were calculated and shown in Fig. 4(*b*). An increase in the Ti content leads to a significant increase in the hardness. The pure MoS_2 coating exhibited the lowest hardness of about 0.2474 GPa, while the MoS_2/Ti-3 composite coating exhibited the highest hardness of 4.902 GPa. Since the structure densification depends on the Ti content, the increased hardness may be explained by the solid solution hardening effect [41]. Figure 4(*c*) presents the relationship between H/E and H^3/E^2 for the four coatings since they are the plastic deformation resistance index of the coating, which reflects the wear resistance of the coating [42,43]. It was observed that the values improve significantly with the increment in the Ti content.

3.3 Fretting Wear Behavior of the Coatings. Figure 5 presents the variation in the coefficient of friction (COF) for the four coatings during the fretting wear test at room temperature. For

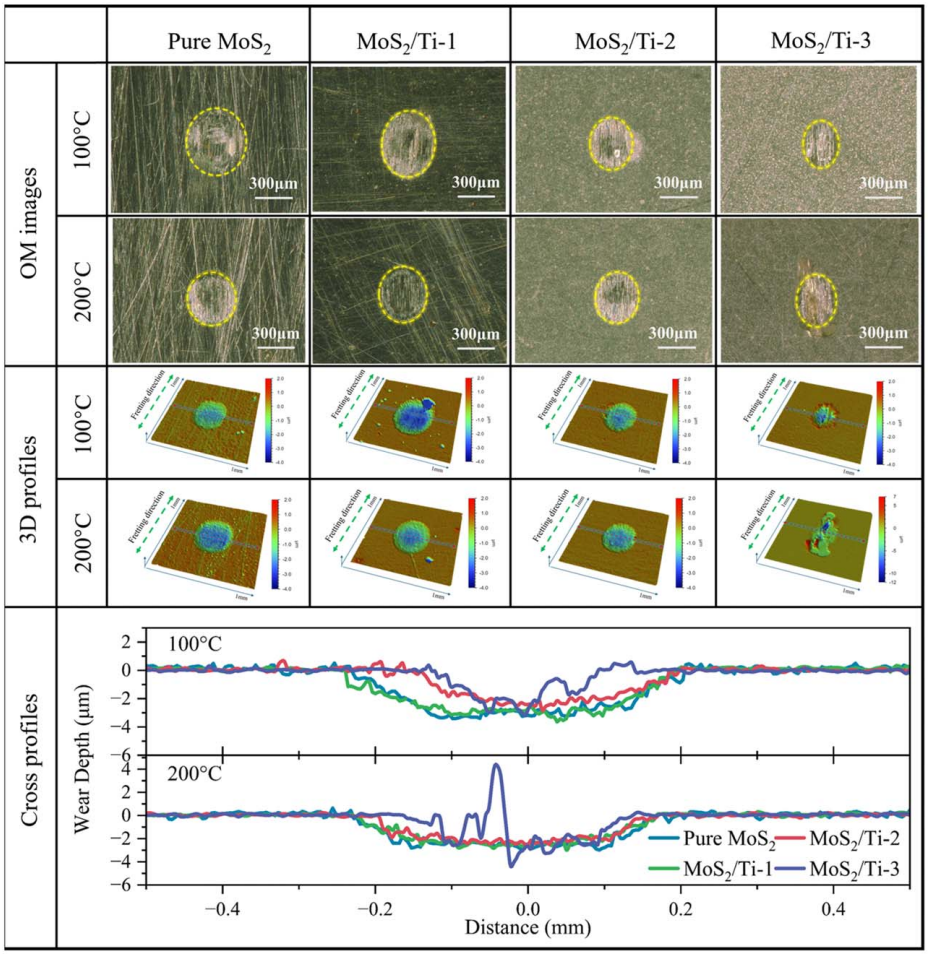

Fig. 8 The optical microscope (OM) images, 3D, and cross-sectional profiles of the wear scars at 100 °C and 200 °C

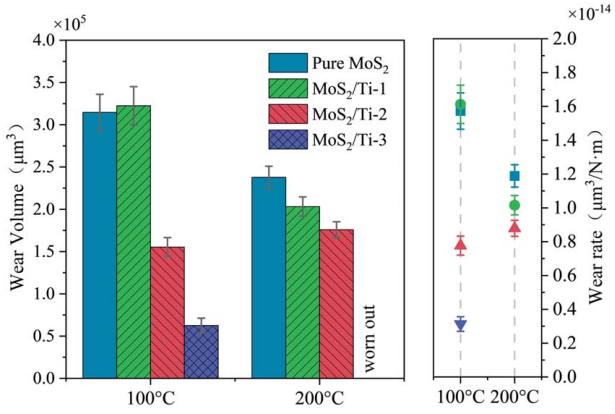

Fig. 9 Wear volume and wear-rate of MoS_2/Ti coatings after fretting wear tests at 100 °C and 200 °C

pure MoS_2 coating, the friction coefficient remained stable at around 0.2 in the first 1000 cycles of the fretting wear process. However, a sharp increase was observed at about 1400 cycles, and it continued to increase up to 0.8 with an increase in number of cycles.

Specimens with a lower Ti content (MoS_2/Ti-1 and MoS_2/Ti-2), exhibited a similar behavior to that of the pure MoS_2. The only difference was in the increased number of cycles till a sharp increase was observed and it was at about 2000 cycles for MoS_2/Ti-1 and at about 3500 cycles for MoS_2/Ti-2. Since it is known that the MoS_2 atomic planes can slip easily because of the low shear strength. However, the loose structure tends to absorb water and oxidize in a humid atmospheric environment, leading to an increased COF [37]. Moreover, during the wear process, the oxidative product of MoO_3 played an anti-lubricating role, resulting in an abrasive effect [44]. Therefore, the COF increased and the service life decreased.

However, MoS_2/Ti-3 coating exhibited a stable COF throughout the 10,000 fretting cycles and no obvious mutation was observed. Moreover, the MoS_2/Ti-3 coating exhibited the lowest COF. The highest hardness with a compact structure of MoS_2/Ti-3 and the highest Ti content may relate to its best anti-fretting wear behavior. Ti and MoS_2 react with oxygen during the wear process, as shown by Eqs. (8) and (9) [45]:

$$Ti + O_2 \rightarrow TiO_2; \quad \Delta G_f^{298} = -888.8\ \text{kJ/mol} \tag{8}$$

$$MoS_2 + O \rightarrow MoO_3; \quad \Delta G_f^{298} = -668.1\ \text{kJ/mol} \tag{9}$$

where ΔG_f^{298} is the reaction Gibbs free energy at 298 K. Since the Gibbs free energy of forming TiO_2 was lower, the oxidation of Ti might have occurred preferentially at room temperature. It means that the incorporation of Ti can protect MoS_2 from oxidizing. The MoS_2/Ti-3 coating with the highest Ti content exhibited the best protective capacity and the lowest COF.

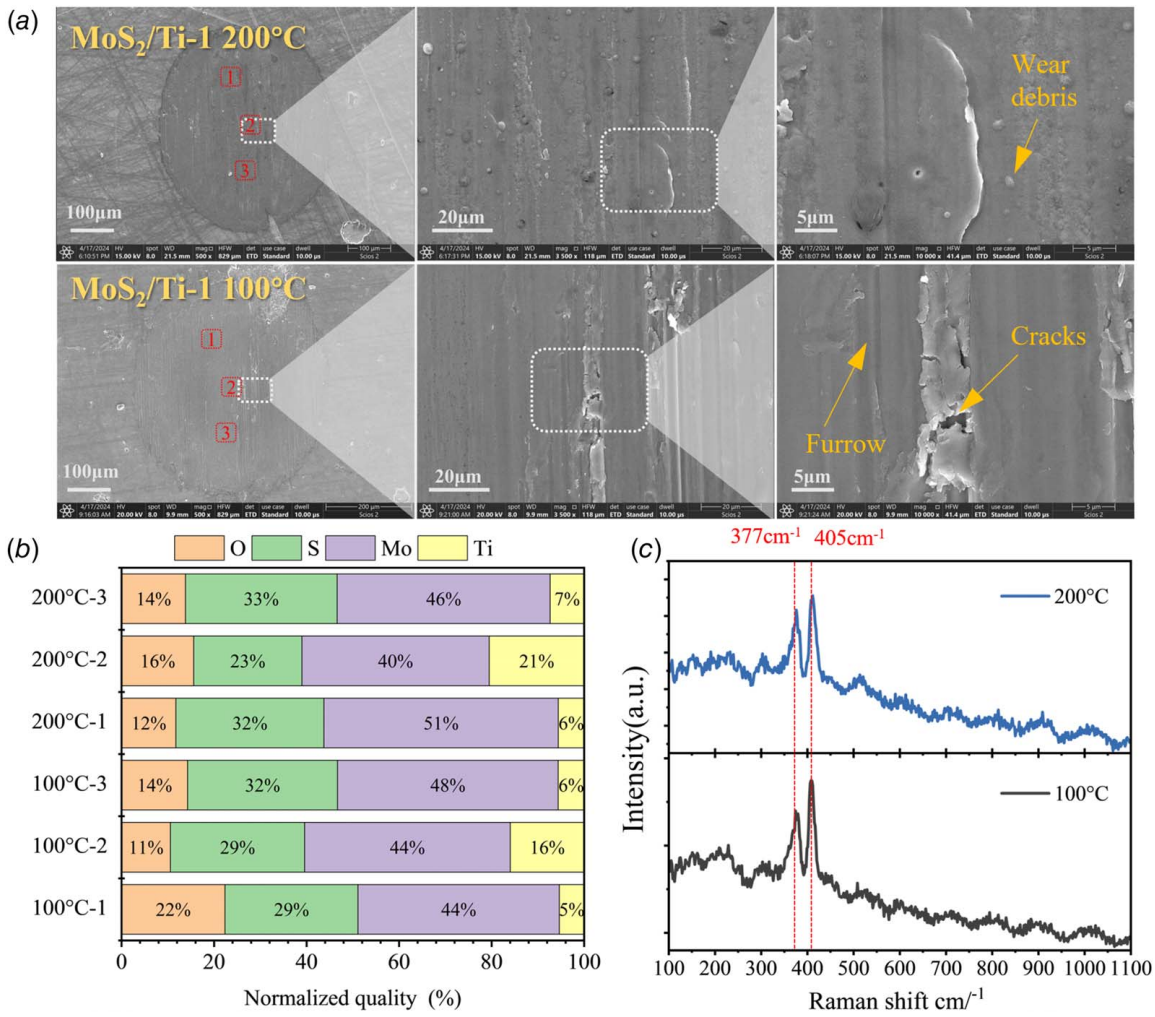

Fig. 10 (*a*) SEM of wear scars, (*b*) EDS, and (c) Raman spectra of MoS_2/Ti-1 coating after 100 °C and 200 °C tests

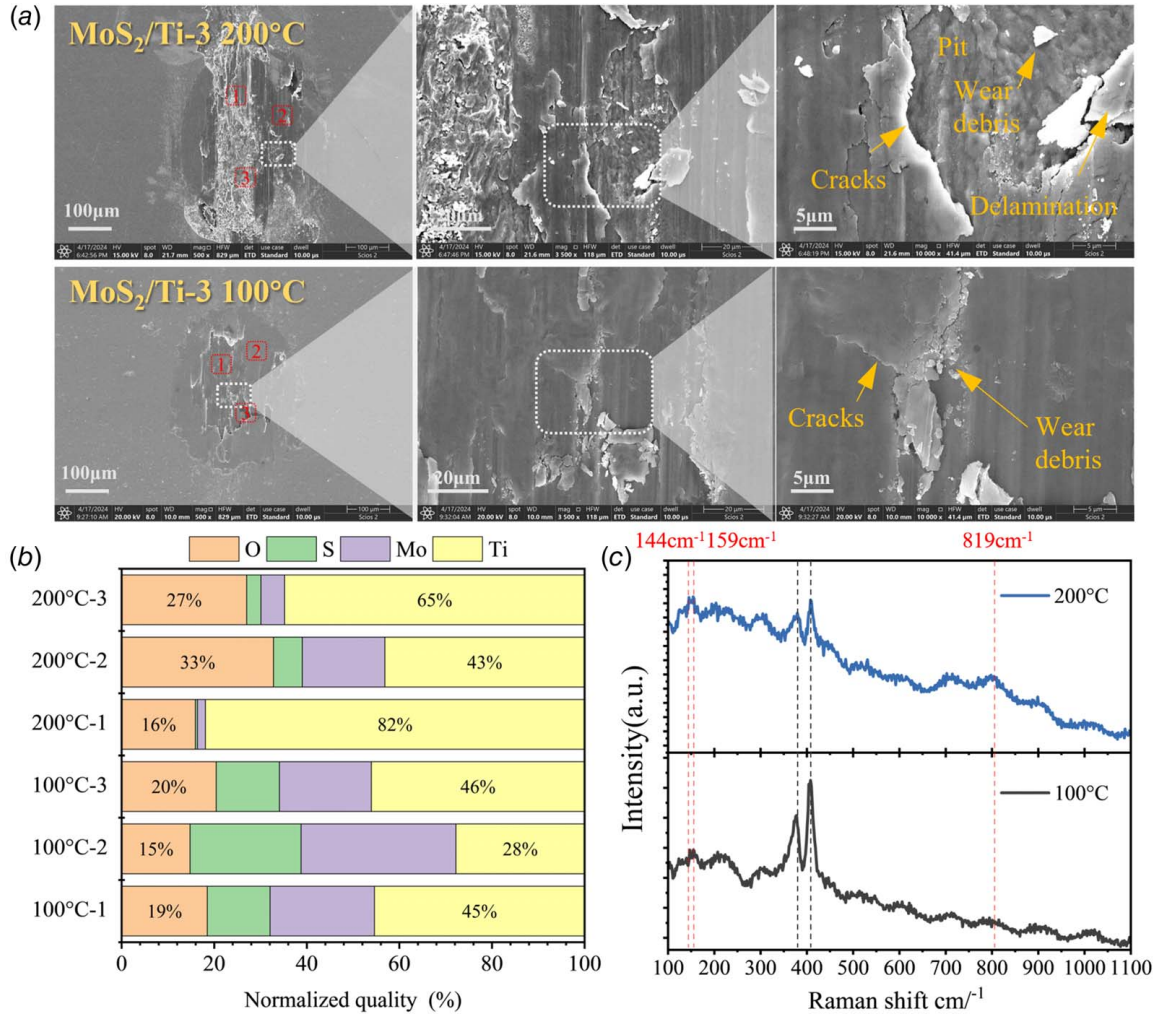

Fig. 11 (*a*) SEM of wear scars, (*b*) EDS, and (c) Raman spectra of MoS_2/Ti-3 coating after 100 °C and 200 °C tests

Figure 6 presents the optical microscope (OM) images, 3D, and cross-sectional profile curves for the four worn coatings. Relatively large wear scars were observed for coatings with low Ti content (MoS_2 and MoS_2/Ti-1), and due to the low hardness, large wear debris forms, repeatedly crushed, refined, and oxidized in the contact area. The agglomeration and sintering of the wear debris lead to the formation of the compacted third-body abrasive dust, which hardly swept away. Such abrasive dust was evident by the protruding cross-sectional profiles. MoS_2/Ti-2 coating exhibited a relatively smaller wear scar, and the wear depth was more than three times of the coating thickness. Based on the wear morphology, it was found that the sudden increase in COF (Fig. 5) resulted from the abrasive dust and the breakthrough of the coating.

However, the MoS_2/Ti-3 coating with the highest Ti content remained relatively intact. The worn surface presented no compacted wear debris and showed the lowest wear depth. Considering the increased ratio of H/E and H^3/E^2 (presented in Fig. 4(*c*)), the coating of MoS_2/Ti-3 demonstrated better anti-fretting wear properties at room temperature.

Figure 7(*a*) presents the variations in the COF for the four coatings at 100 °C and 200 °C. Unlike the room temperature, all the friction curves were found to be stable at high temperatures and exhibited a lower value of COF. Figure 7(*b*) presents the summarized average COF under different temperatures (for the room temperature condition, the friction coefficients before mutation were used). Moreover, MoS_2/Ti coatings with increased Ti content exhibited improved lubrication performance at higher temperatures. The oxidation behavior of MoS_2 was inhibited effectively since the Ti is prone to oxidize. More importantly, the water absorbed between the lamellar structure of MoS_2 was volatilized [46,47], which facilitated the slip behavior of the individual thin atomically planes. Thus, better lubrication behavior of the coatings was achieved at elevated temperatures.

Figure 8 presents the optical microscope images, 3D, and cross-sectional profiles of the wear scars at 100 °C and 200 °C. Coatings with lower Ti content (MoS_2 and MoS_2/Ti-1) exhibited a considerable reduction in wear area and depth at elevated temperatures. However, coatings with higher Ti content exhibited no significant change in wear area and depth. MoS_2/Ti-3 coating, which had the highest Ti content, exhibited film damage at 200 °C.

Figure 9 presents the wear volume and wear-rate of various coatings at 100 °C and 200 °C. A decrease in the wear volume was observed with an increase in temperature for MoS_2 and MoS_2/Ti-1 coatings. However, the coatings with higher Ti content demonstrated the opposite behavior when compared to the results at room temperature.

The worn scars of MoS_2/Ti-1 and MoS_2/Ti-3 coatings were observed by scanning electron microscope (SEM) to further understand the wear mechanism at high temperatures. Figure 10(*a*) presents the microscopic images of the worn surfaces of MoS_2/Ti-1 coating with a low Ti content, while the coating presented uniform and complete wear with visible furrows along the sling direction. Occasional delamination and cracks were also found in the image at a high magnification. For the specimen tested at 200 °C, some tiny fretting particles were found randomly scattered over the worn surface. The sliding of asperity contacts against the

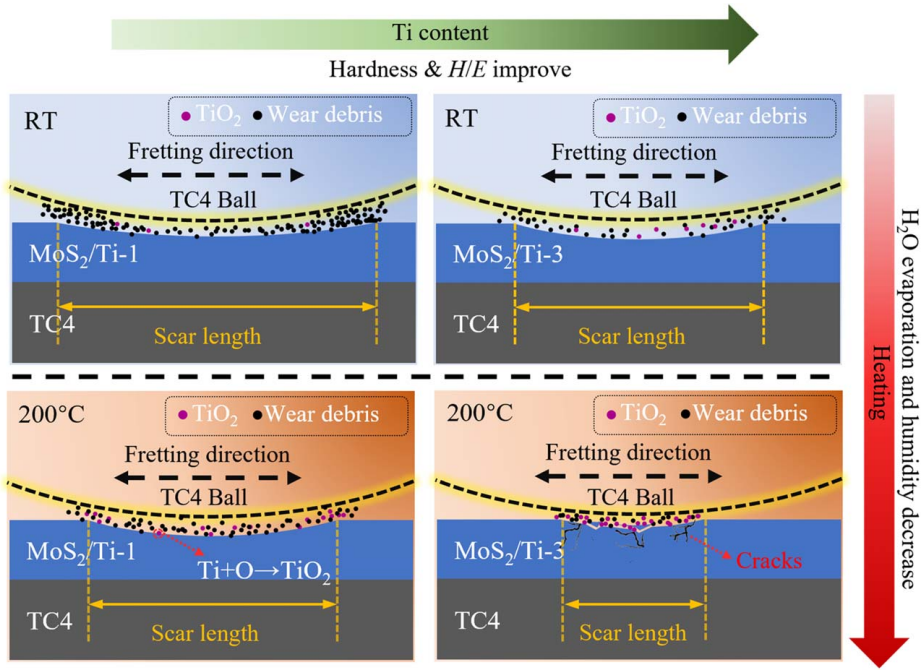

Fig. 12 Schematics of the wear mechanism of MoS_2/Ti coatings with varied Ti contents and temperatures

opposite surface resulted in the breakup of the mechanical interlocking of points on the fretted surfaces. Thus, the fretting debris was generated, which acted as micro-rollers to reduce the COF.

Figure 10(*b*) presents the EDS results at three different positions of the wear scar. Compared with the initial elements Mo, S, and Ti (Table 2), element O was detected on the worn surface, indicating the oxidizing reaction. As can be seen, the Ti content at the center of the wear scars was significantly higher than in the outer regions. This may be attributed to the transfer and accumulation of Ti from the TC4 ball during fretting wear. In addition, the wear scar at the center was deeper and closer to the Ti interlayer. Furthermore, the S content and the ratio of S/Mo in the wear scar showed a slight reduction, as compared with the original coated specimens. Figure 10(*c*) presents the Raman spectroscopy of the wear scars. It exhibited distinct MoS_2 peaks at 377 cm^{-1} and 405 cm^{-1}, corresponding to the E2g and A1g vibrations of MoS_2 layers, respectively [48]. It can be deduced that at elevated temperatures, the improved anti-wear property for MoS_2/Ti-1 coating was mainly attributed to the self-lubricating property of MoS_2.

Figure 11(*a*) presents the worn images of the MoS_2/Ti-3 composite coating with the highest Ti content. Significant scratches and grooves appeared on the wear scar at the 100 °C temperature condition. Under the action of mechanical and thermal stresses, cracks, wear debris, and delamination were observed, which became more intense as the temperature increased up to 200 °C. The presence of severe plastic deformations, larger cracks, and more extensive spalling were observed, as compared with MoS_2/Ti-1. These cracks formed at the surface, penetrated normally to the surface at a short distance and/or subsurface cracks might nucleate and propagate parallel to the surface as suggested by Sporles and Duquette [49]. Another feature of the fretted surface at 200 °C was the presence of shallow pits at the center of the wear scar containing smaller debris. The worn surface outside the pit presented a grooving parallel to the sliding direction, whereas the pit bottom presented no grooving. The boundary between the pit and grooved surface was sharp, typically 3–4 μm in height.

EDS results indicated that the wear scar after the 200 °C test presented more Ti and O contents than 100 °C condition. However, fewer Mo and S elements were also detected, which is quite different from the MoS_2/Ti-1 (Fig. 10(*b*)). From the SEM and EDS analysis, mechanical wear and tribo-oxidation wear were found to be the predominant wear mechanisms. Since MoS_2/Ti-3 contained the highest Ti content and an abundant formation of TiO_2 particles was inevitable at high temperatures according to the Gibbs Free Energy (Eq. (8)). The Raman spectroscopy (Fig. 11(*c*)) presented the characteristic peak of TiO_2 (around 144 cm^{-1}) [50], which depicts the oxidation behavior.

At elevated temperatures, the formation of the oxide debris in fretting occurred due to the oxidation of the fretting surface, followed by the scraping away of this surface oxide or by the oxidation of metallic wear particles. The large number of TiO_2 particles in the frictional interface resulted in abrasive wear and fatigue cracks, promoting the failure of the coatings. Meanwhile, the oxidation was experienced in MoS_2, which can be confirmed by the characteristic peaks of MoO_3 (Fig. 11(*c*), around 159 and 819 cm^{-1}) [51]. A significant reduction in element S was caused by its escape in the form of SO_2 [38] and the consumption of MoS_2 aggravated the wear of the coating.

The effects of the Ti content and temperature on the fretting wear behavior of the MoS_2/Ti coatings are briefly summarized in Fig. 12. The coatings became more denser with an increase in the Ti content and their hardness as well as the *H*/*E* (hardness to elastic modulus) ratio improved. At room temperature, the coating with higher Ti presented better-fretting wear protection based on the decreased wear scar and debris. At elevated temperatures, ambient humidity decreased and H_2O absorbed in the layers of MoS_2 evaporated. Sliding between the MoS_2 layers occurred more easily, while the coatings with moderate Ti content presented better lubrication performance. However, the coatings with the highest Ti contents presented severe wear with poor protective capacity at higher temperatures. Due to the excessive tribo-oxidation, the oxide particles at the frictional interface induce abrasive wear and fatigue cracks.

4 Conclusions

In this research work, the MoS_2/Ti co-deposition coatings were fabricated by using the magnetron sputtering method. The composition, hardness, and elastic modulus of the coatings were evaluated. Fretting wear tests were conducted on the specimens coated with

four coatings, with varying Ti contents and at different temperatures. Following conclusions can be drawn from this research work:

(1) Increase in Ti contents in MoS_2/Ti coatings, results in structure densification, improvement in hardness, and the H/E (hardness to elastic modulus) ratio.
(2) At room temperature, the doped Ti protects the oxidation of MoS_2, and the MoS_2/Ti coating with the highest Ti content maintains a low friction coefficient for the whole test time and exhibits better fretting wear behavior.
(3) At high temperatures, a moderate Ti content of the MoS_2/Ti coating shows better anti-fretting wear properties. However, the coatings with the highest Ti content presented severe wear with poor protective capacity at higher temperatures. Due to the excessive tribo-oxidation, the oxide particles at the frictional interface induce abrasive wear and fatigue cracks.

Acknowledgment

The authors thank the support by National Key Laboratory of Helicopter Aeromechanics Funding (2024-CXPT-GF-JJ-093-03), National Key Laboratory of Science and Technology on Helicopter Transmission (Grant No. HTL-A-22G14), and Fundamental Research Funds for the Central Universities (3082023NS2023025).

Conflict of Interest

There are no conflicts of interest.

Data Availability Statement

The datasets generated and supporting the findings of this article are obtainable from the corresponding author upon reasonable request.

References

[1] Fouvry, S., Paulin, C., and Deyber, S., 2009, "Impact of Contact Size and Complex Gross–Partial Slip Conditions on Ti–6Al–4V/Ti–6Al–4V Fretting Wear," Tribol. Int., **42**(3), pp. 461–474.
[2] Wang, L., Ding, H. Y., Liu, A. H., and Wang, S., 2017, "Wear Performance of TC4 Alloys in Different Tribo-Systems," Rare Metal Mater. Eng., **46**(9), pp. 2449–2454.
[3] Zhao, Q. Y., Yu, T. X., Pang, T. Y., and Song, B. F., 2022, "Spline Wear Life Prediction Considering Multiple Errors," Eng. Fail. Anal., **131**(4), p. 105804.
[4] Zhang, F. T., Liang, Y. L., Wu, Y. Z., Yin, C., Zhang, J., Yang, S., and Huang, X., 2022, "Microstructure Evolution of a Drive Shaft Spline From an Aero-Engine Fuel Pump During Fretting Wear," Mater. Res. Express, **9**(4), p. 6513.
[5] Xiao, L., Xu, Y. Q., Sun, X. W., Xu, H., and Zhang, L., 2022, "Experimental Investigation on the Effect of Misalignment on the Wear Failure for Spline Couplings," Eng. Fail. Anal., **131**(1), p. 105755.
[6] Fouvry, S., Arnaud, P., Mignot, A., and Neubauer, P., 2017, "Contact Size, Frequency and Cyclic Normal Force Effects on Ti–6Al–4V Fretting Wear Processes: An Approach Combining Friction Power and Contact Oxygenation," Tribol. Int., **113**(1), pp. 460–473.
[7] Yang, Q., Zhou, W. L., Zhong, Y. N., Zhang, X., Fu, X., Chen, G., and Li, Z., 2018, "Effect of Shot-Peening on the Fretting Wear and Crack Initiation Behavior of Ti–6Al–4V Dovetail Joint Specimens," J. Mater. Res. Technol., **107**(1), pp. 83–95.
[8] Yang, Q., Zhou, W. L., Niu, Z. Q., Zheng, X., Wang, Q., Fu, X., Chen, G., and Li, Z., 2018, "Effect of Different Surface Asperities and Surface Hardness Induced by Shot-Peening on the Fretting Wear Behavior of Ti–6Al–4V," Surf. Coat. Technol., **349**(1), pp. 1098–1106.
[9] Fridrici, V., Fouvry, S., and Kapsa, P., 2001, "Effect of Shot Peening on the Fretting Wear of Ti–6Al–4V," Wear, **250**(1), pp. 642–649.
[10] Sharma, A., and Sadeghi, F., 2024, "Effects of Fretting Wear on Rolling Contact Fatigue," Tribol. Int., **192**(1), p. 109204.
[11] Wang, Z. H., Lu, Y. H., Zhang, H. Y., and Shoji, T., 2016, "Effect of Cold Rolling on the Fretting Wear Behavior and Mechanism in Inconel 600 Alloy," Tribol. Trans., **59**(5), pp. 923–931.
[12] Sun, D. J., Wu, X. Q., Xie, F. Q., He, P., Li, Z., and He, J., 2023, "Fretting Wear Properties and Microstructure Evolution in Micro-Arc Oxidation Bioceramic Coating Pretreated Using Laser Remelting," Ceram. Int., **49**(3), pp. 4979–4986.
[13] Lai, P., Zhang, H., Zhang, L. F., Zeng, Q., Lu, J., and Guo, X., 2019, "Effect of Micro-Arc Oxidation on Fretting Wear Behavior of Zirconium Alloy Exposed to High Temperature Water," Wear, **424**(1), pp. 53–61.
[14] Fridrici, V., Fouvry, S., and Kapsa, P., 2003, "Fretting Wear Behavior of a Cu–Ni–In Plasma Coating," Surf. Coat. Technol., **163**(1), pp. 429–434.
[15] Luo, J., Cai, Z. B., Mo, J. L., Peng, J. F., and Zhu, M. H., 2015, "Torsional Fretting Wear Behavior of Bonded MoS_2 Solid Lubricant Coatings," Tribol. Trans., **58**(6), pp. 1124–1130.
[16] Xu, G. Z. H., Zhu, M. H., Liu, J. J., Zhou, Z., and Liang, H., 2003, "The Effect of Pre-Treatment of Substrate on Fretting Tribological Behavior of MoS_2 Coatings," Wear, **255**(1), pp. 246–252.
[17] Zhou, J. B., Zhang, L., Ding, Y., Chen, X., and Cai, Z., 2021, "Impact Fretting Wear of MoS_2/C Nanocomposite Coating With Different Carbon Contents Under Cycling low Kinetic Energy," Nanomaterials, **11**(9), p. 2205.
[18] Zhuang, W. H., Li, H., Li, W., Fan, X., He, J., Cai, Z., Fu, W., Zhang, G., Wan, S., and Zhu, M., 2019, "Probing Fretting Performance of DLC and MoS_2 Films Under Fluid Lubrication," Appl. Surf. Sci., **478**(1), pp. 661–679.
[19] Zhang, Y. Y., Descartes, S., Vo, P., and Chromik, R. R., 2016, "Cold-Sprayed Cu–MoS_2 and Its Fretting Wear Behavior," J. Therm. Spray Technol., **25**(3), pp. 473–482.
[20] Wang, P., Zhang, G. G., Lu, Z. B., Yue, W., and Zhu, L., 2019, "Effect of Electric Currents on Tribological Behaviors of Ti/MoS_2 Composite Film Sliding Against Aluminum," Surf. Topogr. Metrol. Prop., **7**(2), p. 025014.
[21] Weise, G., Mattern, N., Hermann, H., Teresiak, A., Bächer, I., Brückner, W., Bauer, H.-D., et al., 1997, "Preparation, Structure and Properties of MoSx Films," Thin Solid Films, **298**(1–2), pp. 98–106.
[22] Corbella, C., Portal, S., Kundrapu, M. N., and Keidar, M., 2022, "Nanosynthesis by Atmospheric arc Discharges Excited with Pulsed-DC Power: A Review," Nanotechnology, **33**(34), p. 342001.
[23] Kononov, A. A., Castro-Arata, R. A., Glavnaya, D. D., Stozharov, V. M., Dolginsev, D. M., Saito, Y., Fons, P., Anisimova, N. I., and Kolobov, A. V., 2020, "Polarization Processes in Thin Layers of Amorphous MoS_2 Obtained by RF Magnetron Sputtering," Semiconductors, **54**(5), pp. 558–562.
[24] Vierneusel, B., Schneider, T., Tremmel, S., Wartzack, S., and Gradt, T., 2013, "Humidity Resistant MoS_2 Coatings Deposited by Unbalanced Magnetron Sputtering," Surf. Coat. Technol., **235**(1), pp. 97–107.
[25] Yin, J. N., Yue, Z. F., Fan, X. Q., Zhuang, W., and Zhu, M., 2023, "Study on the Effect of Counter Ball Materials on Fretting Wear Behavior of Solid Lubricating Films," Wear, **526**(1), p. 204957.
[26] Mukhtar, S. H., Wani, M. F., Sehgal, R., and Sharma, M. D., 2023, "Nano-Mechanical and Nano-Tribological Characterisation of Self-Lubricating MoS_2 Nano-Structured Coating for Space Applications," Tribol. Int., **178**(1), p. 108017.
[27] Kraut, D., Weise, G., Olbrich, W., and Kampschulte, G., 1993, "Low-Friction Composite Coating of Crxsiy MoS_2 on Steel," Surf. Coat. Technol., **60**(1–3), pp. 515–520.
[28] Bhattacharya, R. S., Rai, A. K., Mccormick, A. W., and Erdemir, A., 1993, "High-Enegry (MEV) Ion-Beam Modifications of Sputtered MoS_2 Coating on Creamics," Tribol. Trans., **36**(4), pp. 621–626.
[29] Zaharin, H. A., Ghazali, M. J., Thachnatharen, N., Ezzah, F., Walvekar, R., and Khalid, M., 2023, "Progress in 2D Materials Based Nanolubricants: A Review," Flatchem, **38**(1), p. 100485.
[30] Teer, D. G., Hampshire, J., Fox, V., and Bellido-Gonzalez, V., 1997, "The Tribological Properties of MoS_2/Metal Composite Coatings Deposited by Closed Field Magnetron Sputtering," Surf. Coat. Technol., **94–95**(1–3), pp. 572–577.
[31] Shi, X., He, P., Sun, S., Chen, J., Beake, B. D., Liskiewicz, T. W., Zhang, X., and Zhou, Z., 2022, "Tailoring the Corrosion and Tribological Performance of Ti-Modified MoS_2-Based Films in Simulated Seawater," J. Mater. Res. Technol., **21**(1), pp. 576–589.
[32] Li, H., Zhang, G., and Wang, L., 2016, "Low Humidity-Sensitivity of MoS_2/Pb Nanocomposite Coatings," Wear, **350–351**(1), pp. 1–9.
[33] Sun, J. Y., Weng, L. J., Yu, D. Y., and Xue, Q., 2002, "RF-Sputtered REMF–MoS_2–Au/Au Nanocomposite Multilayer Film," Vacuum, **65**(1), pp. 51–58.
[34] Wang, Y., Li, R., Zhao, X., Xue, Y., An, Y., Zhou, H., and Chen, J., 2023, "The Synergistic Action of Ag and MoS_2 on Tribological Properties of Al_2O_3/Ag(MoS_2) Composite Coatings," Surf. Coat. Technol., **466**(1), p. 129633.
[35] Lu, X., Yan, M., Yan, Z., Chen, W., Sui, X., Hao, J., and Liu, W., 2021, "Exploring the Atmospheric Tribological Properties of MoS_2–(Cr, Nb, Ti, Al, V) Composite Coatings by High Throughput Preparation Method," Tribol. Int., **156**(1), p. 106844.
[36] Hu, Y., Wang, J. J., Li, W., Tang, X., Tan, T., Li, Z., Feng, H., and Zhang, G., 2024, "The Effects of Ti Content on Tribological and Corrosion Performances of MoS_2–Ti Composite Films," Vacuum, **221**(1), p. 112889.
[37] Serpini, E., Rota, A., Ballestrazzi, A., Marchetto, D., Gualtieri, E., and Valeri, S., 2017, "The Role of Humidity and Oxygen on MoS_2 Thin Films Deposited by RF PVD Magnetron Sputtering," Surf. Coat. Technol., **319**(1), pp. 345–352.
[38] Khare, H. S., and Burris, D. L., 2014, "Surface Andsubsurface Contributions of Oxidation and Moisture to Room Temperature Friction of Molybdenum Disulfide," Tribol. Lett., **53**(1), pp. 329–336.
[39] Zhou, H., Zheng, J., Wen, Q. P., Wan, Z.-H., and Sang, R.-P., 2011, "The Effect of Ti Content on the Structural and Mechanical Properties of MoS_2–Ti Composite Coatings Deposited by Unbalanced Magnetron Sputtering System," 4th International Conference on Surface and Interface Science and Engineering (SISE), Lanzhou, China, Sept. 12–18.
[40] Oliver, W. C., and Pharr, G. M., 1992, "An Improved Technique for Determining Hardness and Elastic Modulus Using Load and Displacement Sensing Indentation Experiments," J. Mater. Res. Technol., **7**(6), pp. 1564–1583.
[41] Renevier, N. M., Lobiondo, N., Fox, V. C., Teer, D. G., and Hampshire, J., 2000, "Performance of MoS_2metal Composite Coatings Used for Dry Machining and Other Industrial Applications," Surf. Coat. Technol., **123**(1), pp. 84–91.

[42] Chen, X., Du, Y., and Chung, Y.-W., 2019, "Commentary on Using H/E and H^3/E^2 as Proxies for Fracture Toughness of Hard Coatings," Thin Solid Films, **688**(1), p. 137265.
[43] Beake, B. D., 2022, "The Influence of the H/E Ratio on Wear Resistance of Coating Systems—Insights From Small-Scale Testing," Surf. Coat. Technol., **442**(1), p. 128272.
[44] Qin, X. P., Ke, P. L., Wang, A. Y., and Kim, K. H., 2013, "Microstructure, Mechanical and Tribological Behaviors of MoS_2–Ti Composite Coatings Deposited by a Hybrid HIPIMS Method," Surf. Coat. Technol., **228**(1), pp. 275–281.
[45] Dean, J. A., 1978, *Lange's Handbook of Chemistry*, McGraw-Hill, New York.
[46] Zeng, C., Pu, J. B., Wang, H. X., Zheng, S., Wang, L., and Xue, Q., 2019, "Study on Atmospheric Tribology Performance of MoS_2-W Films With Self-Adaption to Temperature," Ceram. Int., **45**(13), pp. 15834–15842.
[47] Pritchard, C., and Midgley, J. W., 1969, "The Effect of Humidity on the Friction and Life of Unbonded Molybdenum Disulphide Films," Wear, **13**(1), pp. 39–50.
[48] Li, H., Li, X., Zhang, G. A., Wang, L., and Wu, G., 2017, "Exploring the Tribophysics and Tribochemistry of MoS_2 by Sliding MoS_2/Ti Composite Coating Under Different Humidity," Tribol. Lett., **65**(2), p. 38.
[49] Sproles, E. S., and Duquette, D. J., 1978, "The Mechanism of Material Removal in Fretting," Wear, **49**(2), pp. 339–352.
[50] Wang, K.-X., Wang, X.-Y., Hong, C.-B., Zhao, B.-Y., Xie, W.-C., and Tang, W.-Q., 1995, "Raman Studies on Nanocrystal TiO_2 Gels," Acta Phys. -Chim. Sin., **11**(1), pp. 5–8.
[51] Wang, Y., Du, X., Wang, J., Su, M., Wan, X., Meng, H., Xie, W., Xu, J., and Liu, P., 2017, "Growth of Large-Scale, Large-Size, Few-Layered α-MoO_3 on SiO_2 and Its Photoresponse Mechanism," ACS Appl. Mater. Interfaces, **9**(6), pp. 5543–5549.